AD-A092 473 NAVAL RESEARCH LAB WASHINGTON DC F/G 11/6
EFFECT OF STRESS-STRAIN BEHAVIOR ON LOW-CYCLE FATIGUE OF ALPHA---ETC(U)
NOV 80 J M KRAFFT
UNCLASSIFIED NRL-MR-4406 NL

1 OF 1
AD A 092 473

END
DATE FILMED
1-81
DTIC

SECURITY CLASSIFICATION OF THIS PAGE (When Data Entered)

REPORT DOCUMENTATION PAGE

READ INSTRUCTIONS BEFORE COMPLETING FORM

1. REPORT NUMBER: NRL Memorandum Report 4406
2. GOVT ACCESSION NO.: AD-A092 473
3. RECIPIENT'S CATALOG NUMBER:

4. TITLE (and Subtitle): EFFECT OF STRESS-STRAIN BEHAVIOR ON LOW-CYCLE FATIGUE OF α-β TITANIUM ALLOYS

5. TYPE OF REPORT & PERIOD COVERED: Interim report on a continuing NAIR and NRL problems.

6. PERFORMING ORG. REPORT NUMBER:

7. AUTHOR(s): J. M. Krafft

8. CONTRACT OR GRANT NUMBER(s):

9. PERFORMING ORGANIZATION NAME AND ADDRESS: Naval Research Laboratory, Washington, D.C. 20375

10. PROGRAM ELEMENT, PROJECT, TASK AREA & WORK UNIT NUMBERS: 58-0263-0-1; RR023-03-45; 58-0264-0-1; WR022-01-01

11. CONTROLLING OFFICE NAME AND ADDRESS: Naval Research Laboratory, Washington, D.C. 20375

12. REPORT DATE: November 21, 1980

13. NUMBER OF PAGES: 29

14. MONITORING AGENCY NAME & ADDRESS(if different from Controlling Office):

15. SECURITY CLASS. (of this report): UNCLASSIFIED

15a. DECLASSIFICATION/DOWNGRADING SCHEDULE:

16. DISTRIBUTION STATEMENT (of this Report)

Approved for public release; distribution unlimited.

17. DISTRIBUTION STATEMENT (of the abstract entered in Block 20, if different from Report)

18. SUPPLEMENTARY NOTES

19. KEY WORDS (Continue on reverse side if necessary and identify by block number)

Low Cycle Fatigue
Cyclic Strain Hardening
Titanium Alloys
Creep Fatigue Interaction

20. ABSTRACT (Continue on reverse side if necessary and identify by block number)

In earlier NRL work, Ti-6Al-4V in four levels of interstitial oxygen content and a single Ti-8Al-1Mo-1V alloy plate were heat treated to alter grain size and/or microstructural character; the effect on fatigue crack propagation rate was measured. In this work, small tensile specimens of these materials are subjected to slow strain-controlled cyclic deformation leading to rupture in the 5-500 cycle range. Indication of crack initiation as well as rupture life are compared relative

(Continued)

DD FORM 1 JAN 73 1473 EDITION OF 1 NOV 65 IS OBSOLETE
S/N 0102-014-6601

20. ABSTRACT (Continued)

to the plastic excursion strain. On this basis, effects of grain size and oxygen content are not clearly discriminated. Yet, some of the materials exhibit markedly superior performance. This improvement seems to be related to a characteristic evolution in the shape of the cyclic stress-strain curve. Here, relative to a full convex hysteresis loop of early cycles, the later cycles exhibit a reduced stress level, or cyclic softening, in the first half of the excursion, followed by a resurgence of strength to initial stress levels in the latter portion. The enhanced strain hardening rate enabling this terminal strength restoration is thought to stabilize the deformation, reducing the amount of stress-relaxation-induced tensile strain. Taking such strain as an increment of damage in a cumulative cyclic creep strain criterion provides a correlation between the evolving shape of the cyclic stress-strain curve and the low cycle fatigue endurance. Results indicate the absolute increase in the terminal plastic strain hardening rate to be a constant of a material, independent of the cyclic strain excursion.

CONTENTS

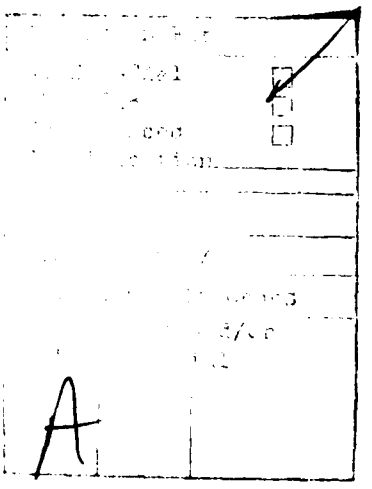

EFFECT OF STRESS-STRAIN BEHAVIOR ON LOW-CYCLE FATIGUE OF α–β TITANIUM ALLOYS

1. INTRODUCTION

The fatigue behavior of titanium alloys often governs the service interval between inspections of aircraft jet engines in which it is used for blades and rotors in fan and compressor stages. Here the resistance to crack initiation is basic, as the fatigue life of a part is set in terms of the probability of initiating a small surface crack. The subsequent crack propagation life is important, nonetheless, as a final period of grace before catastrophic failure. Both measure of fatigue resistance can be influenced by metallurgical variables. Unfortunately, changes in metallurgical factors which improve some characteristics typically work to the detriment of others. Thus, a remarkable improvement in resistance to fatigue crack growth was discovered by Yoder, Cooley and Crooker [1,2,3], who found that increased grain size in alpha/beta titanium alloys produced order-of-magnitude reductions in crack growth rate, with less than expected reduction in strength properties. A penalty is suggested, however, by data on other alloy systems, where increased grain size adversely affects fatigue crack initiation life: work of Feltner and Beardmore on copper [4], Boettner, Laird and McEvily on aluminum alloys [5], Abdel-Raouf, Topper and Plumtree on iron [6]. Interstitial oxygen, as an alpha phase stabilizer, tends to increase strength but degrade ductility and fracture resistance. In unalloyed titanium, Beevers and Robinson [7] find oxygen content to increase fatigue life relative to applied stress. In alpha/beta structural alloys, however, its influence is uncertain. This paper reports part of an ongoing NRL effort to assess the roles of grain size and oxygen content on fatigue crack initiation, using strain controlled low cycle fatigue endurance as the measure of performance.

Manuscript submitted on October 17, 1980.

2. MATERIALS AND HEAT TREATMENT

The titanium alloys were procured for the earlier crack propagation tests [1,2,3] in the form of 25.4 mm thick rolled plate, with chemical analyses as given in Table I. Heat treatment was performed in a vacuum furnace following the schedules shown in Table II. Resulting mechanical properties are listed in Table III where some parameters resulting from fatigue modeling to follow are also included.

3. TEST METHOD

Small cylindrically-sectioned dumbbell-shaped tensile specimens were cycled under total strain control in an alignment subpress of a screw driven testing machine. Specimens and procedures are within general guidelines of the ASTM Test Method 606 [8]. However, the tensile specimens are scaled down to be short enough to permit excisement normal the fracture plane of a broken remnant of a 1-T compact tension specimen CTS of ASTM E399 [9]. This permits direct identification of the test material with that of earlier crack propagation testing on CTS type specimens. The specimen is of cylindrical section, 4.32 mm (0.170 in) diameter, about 9 mm (0.35 in) length between fillets, which flare outward to 12.7 mm threaded buttons. Most test sections were finished with a fine lathe cut, then rotationally smoothed with 400 grade abrasive paper, followed by polishing with a fine aluminum oxide abrasive powder. Comparison of endurances with polished vs machined-only surfaces showed little if any difference; hence data with both finishes is intermixed here.

Table I — Chemical Analyses

Alloy	Content (wt-%)								
	O	Al	Mo	V	Fe	N	C	H	Al*
Ti-8-1-1	0.11	7.8	1.0	1.0	0.11	0.015	0.03	0.0046	
Ti-6-4	0.06	6.0	—	4.1	0.05	0.008	0.023	0.0050	7.0
Ti-6-4	0.11	6.1	—	4.0	0.18	0.009	0.02	0.0069	7.6
Ti-6-4	0.18	6.6	—	4.4	0.20	0.014	0.02	0.0058	8.9
Ti-6-4	0.20	6.7	—	4.3	0.10	0.011	0.03	0.0060	9.2

Note: Al* is the aluminum equivalent

$$Al^* = Al + \frac{Sn}{3} + \frac{Zr}{3} + 10\,(O + C + 2N).$$

Table IIA — Heat Treatments for Ti-8Al-1Mo-1V

Heat Treatment Code	Heat Treatment Type	Specification*
1a	DA	(913°C/1 h + AC) + (579°C/8 h + AC) + (538°C/2 h + AC)
2.d	BQ	(1093°C/1/2 h + WQ) + (1010°C/1/2 h + AC) + (816°C/1 h + WQ)
2.e	BQ	(1093°C/1/2 h + WQ) + (1010°C/1/2 h + WQ) + (816°C/1 h + WQ)
3.a	BA	(1093°C/1/2 h + AC)
3.b	BA	(1093°C/1/2 h + AC) + 816°C/1 h + AC)
3.c	BA	(1093°C/1/2 h + AC) + (1010°C/1/2 H + AC) + (816°C/1 h + AC)
3.d	BA	(1093°C/1/2 h + AC) + (1010°C/1/2 H + AC) + (816°C/1 h + WQ)
3.e	BA	(1093°C/1/2 h + AC) + (1010°C/1/2 H + WQ) + (816°C/1 h + WQ)
4	A"	(1093°C/1/2 h + AC) + (921°C/1 h + WQ)
5	RB	(1093°C/1/2 h + AC) + (849°C/2 + WQ)
6	dB	(1093°C/6 h + AC) + (1093°C/6 + AC) + (816°C/1 h + AC)

Table IIB — Heat Treatments for Ti-6Al-4V

Heat Treatment Type	Specification*
MA	788°C, 1 h /AC (as received)
RA	954°C, 4 h/HC @ 180°C/h to 760°C/AC @ 370°C/h to 482°C/AC
BA	1038°C, 0.5 h/HC to RT + 732°C, 2 h/AC

*Anneals performed in vacuum furnace; h = hour, WQ = water quench, FC = furnace cool, AC = cooled in He @ approx. air cooling rate

Table III — Mechanical Properties

Alloy		Heat Treatment		Orientation	0.2% Yield Strength σ_y	Tensile Strength σ_{uts}	Young's Modulus E	Reduction in Area	Elongation*	Effective Grain Size $\bar{l}$	ISH $\Delta\theta_i$	$\frac{Ni}{\bar{L}}$	Stress Relax. Expon.	Ni $\sum_0^L \Delta\epsilon_c$
	Wt-% Oxygen	No.	Type		(MPa)	(MPa)	(GPa)	(%)	(%)	(μm)	(GPa)	(cycles)	m	(%)
Ti-8-1-1	0.11	1	DA	T	958	1025	136	20	13	9				
Ti-8-1-1	0.11	2.d	BQ	T	840	952	125	13	11					
Ti-8-1-1	0.11	2.e	BQ	T	862	958	123	16	10					
Ti-8-1-1	0.11	3.a	BA	T	794	894	128	21	11	60				
Ti-8-1-1	0.11			L	803	901	128	20	12					
Ti-8-1-1	0.11	3.b	BA	T	818	895	125	18	10					
Ti-8-1-1	0.11	3.c	BA	T	818	898	128	19	10					
Ti-8-1-1	0.11	3.d	BA	T	809	898	120	19	10					
Ti-8-1-1	0.11	3.e	BA	T	829	933	128	19	9					
Ti-8-1-1	0.11	4	A"	T	774	942	119	19	10					
Ti-8-1-1	0.11	5	RB	T	809	905	117	20	10		15.9	7.0		
Ti-8-1-1	0.11	6	dB	T	809	885	121	20	8					
Ti-6-4	0.20		MA	T	1007	1034	130	29	14	5	7.6	6.0	0.012	0.72
Ti-6-4	0.20		RA	T	931	1007	130	26	15	9	6.2	7.0	0.012	0.84
Ti-6-4	0.20		BA	T	869	958	117	16	11	24	0.3	2.9	0.014	0.41
Ti-6-4	0.18		BA	T	818	906	120	13	8	38	1.4	3.4	0.014	0.48
Ti-6-4	0.11		BA	T	772	869	118	19	10	28	2.1	4.4	0.013	0.57
Ti-6-4	0.06		BA	T	740	818	115	34	10	17	6.2	8.0	0.012	0.96
Ti-6-4	0.06			L	772	829	115	26	10					

*50.8-mm gage length

Axial alignment in the compressive stroke was guided by a cylindrical subpress. Both sliding anvil (25.4 mm diameter) and base contain threaded recesses with square, flat bottoms, against which the specimen was gently torqued to secure alignment, as one of the permissible procedures of ASTM Test Method E606.

Cyclic straining was applied in a 45 KN (10 KIP) Instron testing machine. The subpress was connected, via a 22 KN (5 KIP) load cell, to the lower base. To reduce backlash, the screw driven head was biased upward with heavy coil springs in the manner of Coffin and Tavernelli [10]. A specially designed spherical coupling allowed some translational as well as rotational repositioning at the head-to-anvil junction in both tension and compression.

The Instron was set up to provie a head displacement rate of 0.08 mm/sec (0.2 in/min) providing a constant-load strain rate of 8×10^{-3} sec^{-1}. This slow cycling (about 1/min/cycle) allows ample time for heat dissipation from the specimen and tracking of the recorder; however, it limits the total number of cycles, with reasonable patience, to less than 1000. The effective elastic stiffness of the test assemblage, including a typical titanium specimen, is about 13,000 MPA (2000 ksi).

Most of the tests were monitored by measuring, vs load, the longitudinal extension, using the four-finger clip resistance strain gage instrument shown in an earlier report [11]. Concern that crack initiation might be induced by contact of the hard steel knife edges against the specimen was dispelled by comparison tests using a two-lobed diametral strain gage having smooth broad contact surfaces. The gage length between longitudinal knife edges is about 5 mm, within an effective specimen length of about 10 mm.

Load vs longitudinal displacement was recorded, after appropriate bridge signal amplification, on a Hewlett-Packard X-Y recorder. A reasonable approximation of constant total strain limits was provided by replacing the head displacement limit switches of the Instron with opposing, adjustably spaced micro-switches, actuated by the pen-carriage of the X-Y recorder. In this way, a triangular load vs time wave form was produced, Fig. 1, except for some rounding at the extremities associated with leveling

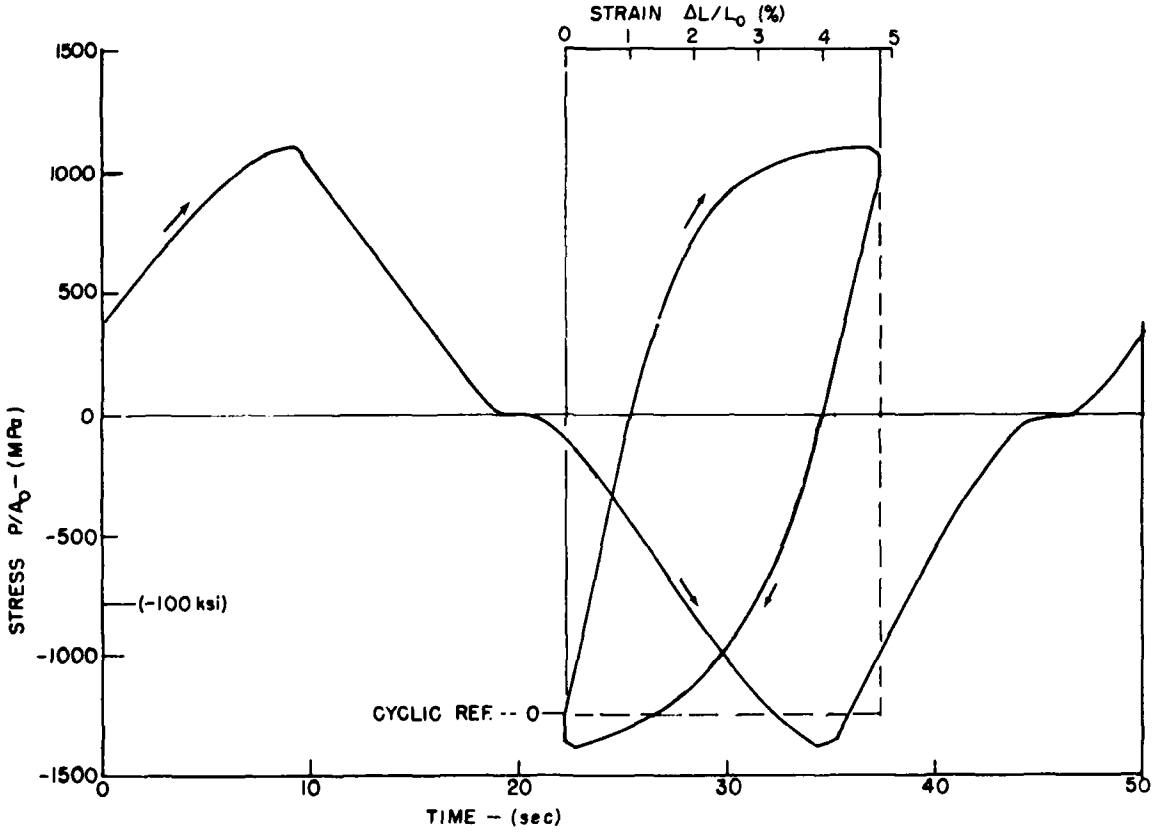

Figure 1 — Typical simultaneous records of stress-time and stress-strain for one LCF cycle

of the stress-strain curve, and consequent increase in strain rate. The switches were set to equalize tensile and compressive total strain excursions about the initial condition. One of the reversing switches was also connected to actuate a cycle-counting relay.

Specimen encumberment by the compression subpress and the strain gage made it difficult to inspect for surface crack initiation. Instead, the cycle count to initiation was estimated by the (usually rapid) transition from a steady cyclic stress-strain shape to a continuously receding one, due to crack growth. Alternatively, the cycle count at a cyclic softening of 10% was used if no earlier indication of crack initiation was evident. In the more propagation-resistant alloys, a collapse of compressive load during crack closure indicates extensive crack initiation [12].

4. LOW CYCLE FATIGUE DATA

The principal data sets are displayed in Fig. 2, showing cycle count to failure (abscissa) against the plastic strain excursion; the leftward bar denotes the estimated point of initiation. In the more propagation-resistant heat treatments, initiation sometimes occurs at less than half the total life. However, in most cases, initiation and rupture are not far apart. This is consistant with observations of Wells and Sullivan [13] for initiation of a macrocrack in Ti-6Al-4V. However they observed microcracks on the scale of the alpha phase grains as early as 5-10% of the fatigue life.

All six of the Ti-6Al-4V grain size/oxygen combinations are shown in Figure 2. For the Ti-8Al-1Mo-1V, the RB heat treatment is shown since it was tested sufficiently to establish a trend. This was done because it was noticed, in running full cyclic stress-strain curves for earlier crack propagation modeling [11], that this heat treatment seemed to effect greater tolerance for cyclic straining than any of the other ten. This singular performance is illustrated in Figure 3, where the RB data from Figure 2 is seen to lie clearly to the right, or longer endurance, of the data band comprising LCF tests for screening all of the ten other heat treatments.

The effect of grain size and of oxygen content is not so neatly distinguished. In the several frames of Figure 2, one can judge performance by the proximity to which the data points approach the

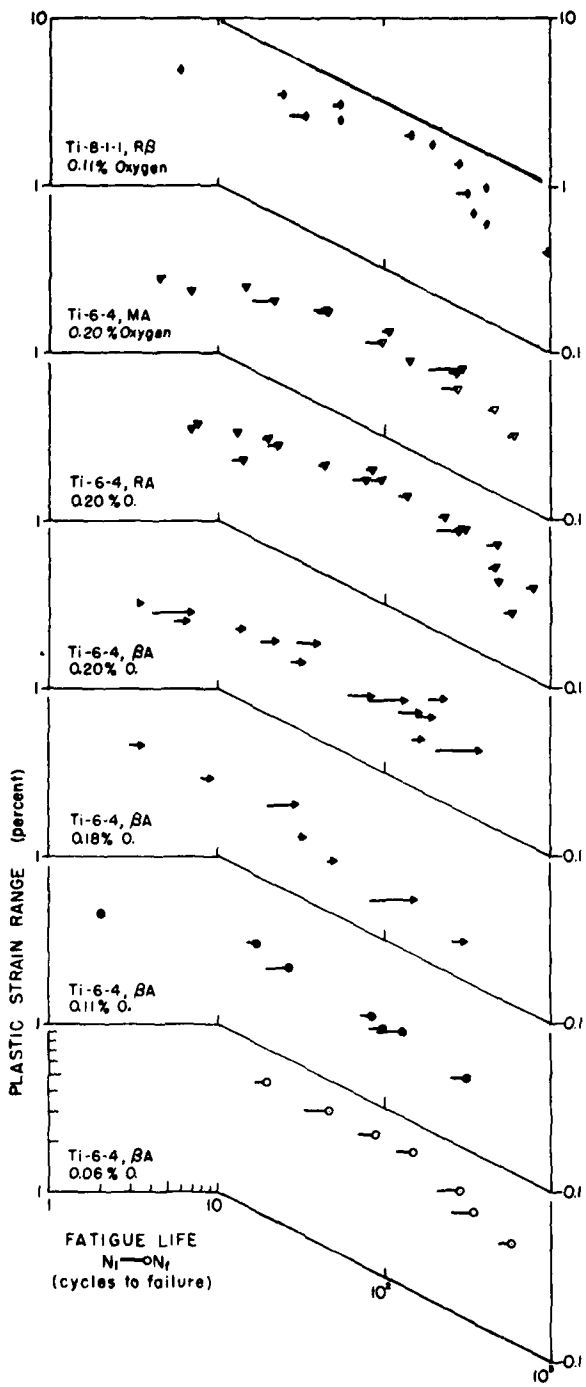

Figure 2 — Fatigue life relative to plastic strain range for the several titanium alloys. Horizontal bar denotes life between crack initiation and final rupture point.

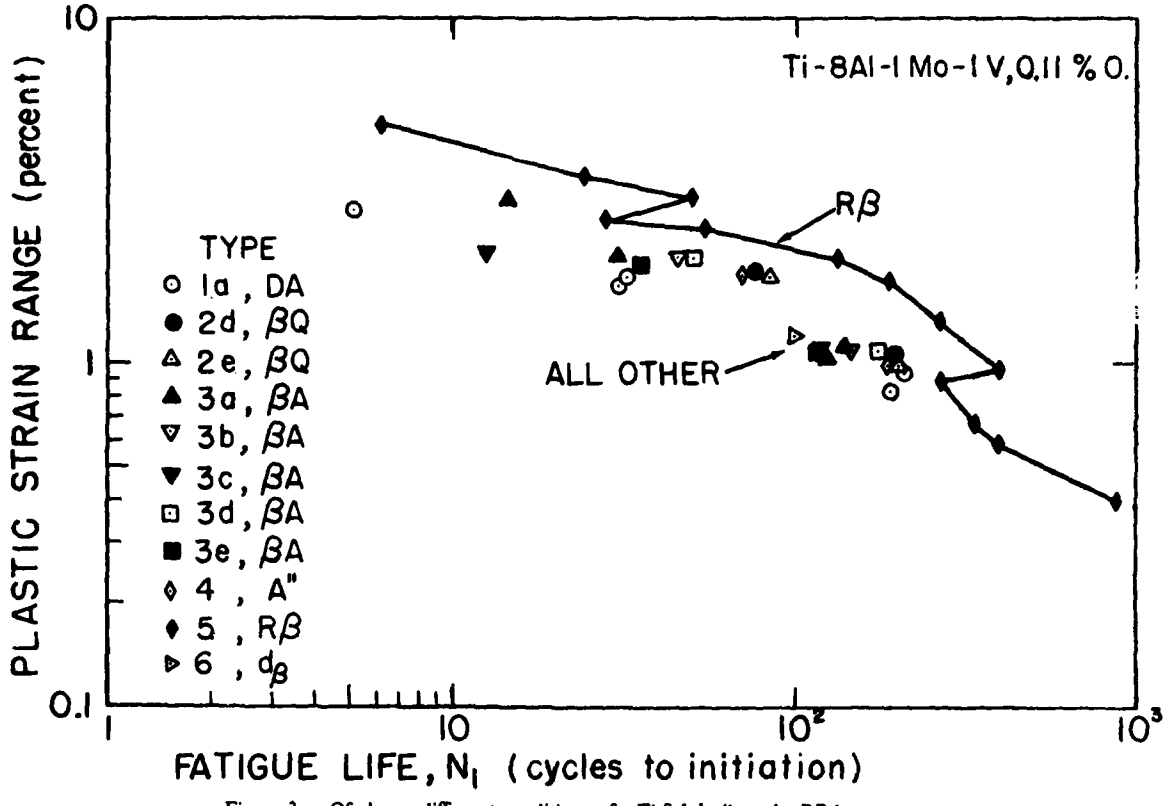

Figure 3 — Of eleven different conditions of a Ti-8-1-1 alloy, the RB heat treatment exhibits exceptional endurance relative to plastic strain excursion

diagonal line between 10%:10 cycles and 1%:1000 cycles as a reference. In this way, the 0.06% oxygen BA is followed closely by 0.20% oxygen RA, thence by 0.20% oxygen MA with other BA alloys of much poorer, generally similar performance. At the same oxygen content, the RA outranks the MA, despite its coarser grain structure and the generally poorer showing of the larger grained, higher oxygen materials. Despite these inconsistencies, certain of the alloys exhibit markedly superior performance, relative to the plastic strain excursion.

5. ANAMALOUS/INVERTED STRAIN HARDENING

In searching for effects with which to associate these improvements in LCF performance, a curious evolution in some of the cyclic stress strain curves was noticed. Initially, the cyclic hysteresis loops exhibit a normal Baushinger effect, a fully convex-outward shape. But as cycling proceeds in some materials, the strain hardening rate appears first to decrease below normal, then increase above it until the loop terminates at about the expected, and little-changed, final stress level. It is as though substantial cyclic softening occurs in the first half of the strain excursion, only to be corrected by cyclic hardening in the latter half. This effect appears to differ from that shown by Stoltz and Pelloux [14] on 2024 aluminum, where, attributed to non-shearable precipitates, the stress dip disappears with continued cycling. It differs too from the increased strain hardening rate found by Richman and Langraf [15], attributed to deformation-induced transformation. With their high carbon steel, both stress and strain hardening rate increased with cycling between fixed total strain limits, and plastic strain decreased. This effect can be distinguished also from onset of specimen cracking, which produces a similar undulation on the compression quadrant as cracks are closed but not in tension [12]. Such cracking reduces the apparent elastic modulus, while the present concavity of the tensile quadrant occurs with no change in modulus. Also, the cracking effect is progressive while the present inverted loop typically holds a steady equilibrium-shape for a large part of the life of a specimen. For convenience in this text, this effect is called Inverted Strain Hardening, with acronym ISH.

Illustrating the range of behaviors, Figure 4 shows hysteresis loop development for three materials, all at about the same 2.5% plastic strain range. Tangent lines fitted to the terminal regions of initial

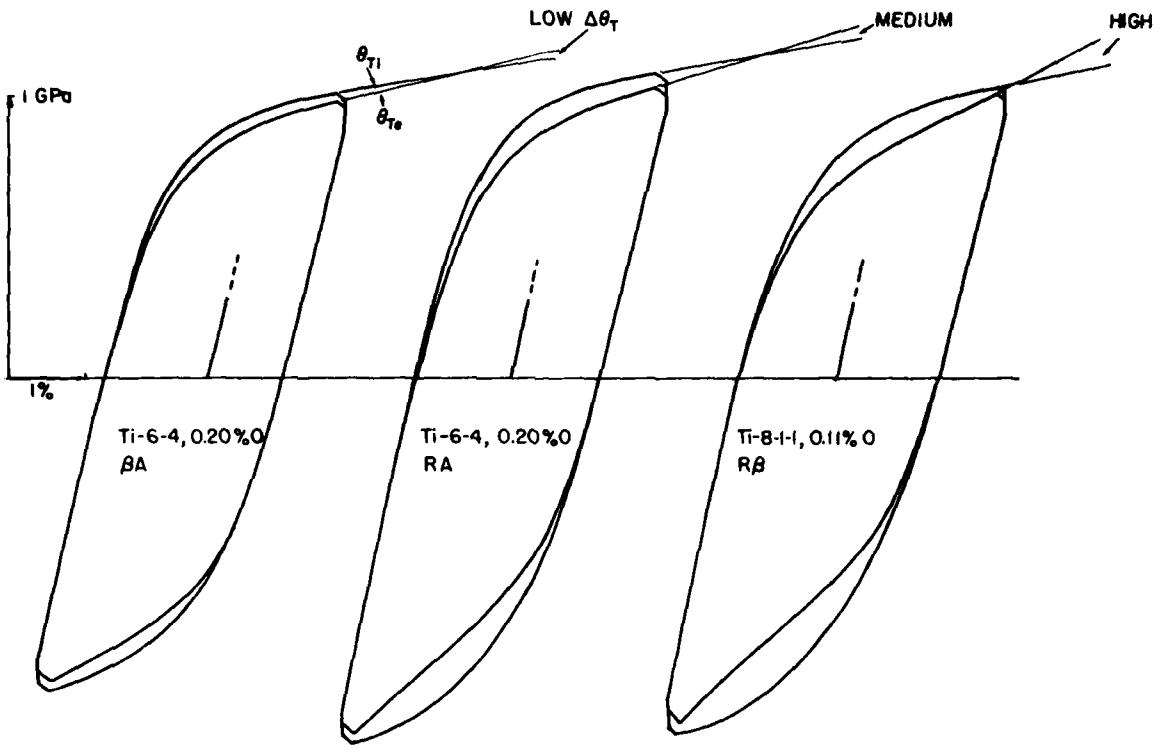

Figure 4 — Varied degrees of inverted strain hardening, ISH, is illustrated by tracings of the tenth vs the third full cycle at about 2-1/2% plastic strain excursion

vs equilibrium loops illustrate the extent of the shift in tangent modulus, hence the strain hardening rate. The two curves traced represent the third and tenth cycle. Three cycles are needed to remove effects of monotonic properties, while ten produces equilibrium short of fracture with this relatively large strain excursion.

In attempt to characterize the ISH effect, initial and equilibrium tangent modulus values, θ_{Ti} and θ_{Te} respectively, were scaled from each of the records. True values were calculated by well known formula [12], assuming constant volume $\nu = 0.5$

$$\theta = \theta_T(1 + \epsilon_T)^2 + \sigma_T(1 + \epsilon_T) \tag{1}$$

$$\theta_p^{-1} = \theta^{-1} - E^{-1} \tag{2}$$

$$\sigma = \sigma_T(1 + \epsilon_T) \tag{3}$$

where θ is the strain hardening rate, ϵ is strain, σ is stress, E is Young's modulus, and subscript T denotes tensile and p plastic values. In Figure 5, values of initial θ_{pi} are plotted vs equilibrium θ_{pe} plastic strain hardening rates for each test; the 1:1 line drawn in provides a base of reference or no change. The data suggests characterization of ISH as an approximately constant value of the increase in θ_p, i.e., $\Delta\theta_p$ = constant, independent of the cyclic strain excursion. When the strain excursion is large, corresponding to low values of θ_p, the full shift may be precluded by specimen rupture, thus tapering the data toward the origin. When the excursion is small, the accuracy is poor in subtracting very large values of θ_p. For intermediate strain excursions, however, the full equilibrium (constant) shift seems to be complete before rupture, and importantly, not precluded by early rupture. To the extent one may assume this, it is notable that alloy conditions leading to improved LCF performance: in Ti-8-1-1, the RB heat treatment; in Ti-6-4, the low oxygen BA, the high oxygen RA and MA; all exhibit a substantial theta-shift with cycling.

6. MODEL FOR EFFECT OF ISH ON LCF

The indication that an upward shift in cyclic strain hardening rate may be associated with greater LCF endurance suggests a connection. The terminal strain hardening rate has a direct influence on the creep strain associated with stress relaxation during the hold time of a fatigue cycle. Cyclic creep strain

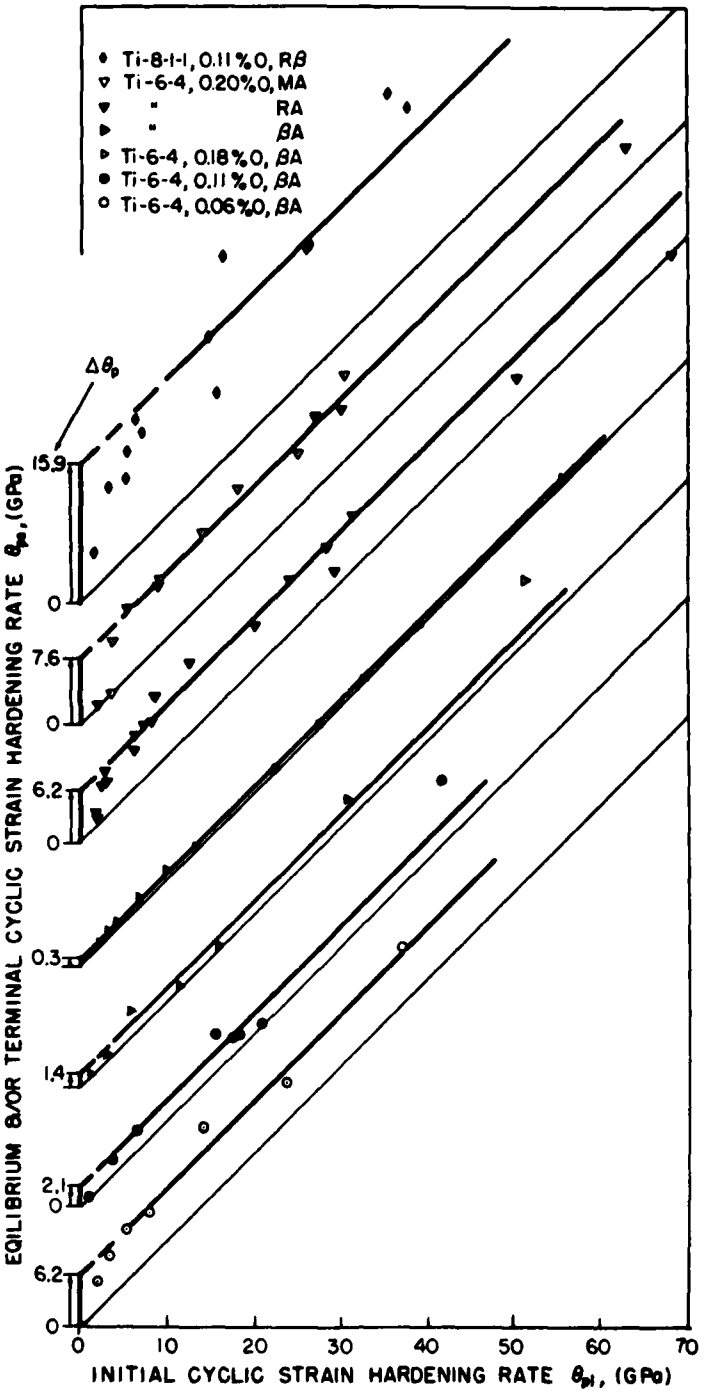

Figure 5 — Plot of equilibrium-vs initial-cyclic true plastic strain-hardening rate suggest a constant degree of change, independent of the strain hardening rate, hence plastic strain excursion.

is a central factor in several theories of creep-fatigue interaction. For example, Serensen, Schneiderovitch and Gussenhov [16] following an idea attributed to Makhutov in 1967, sum the total plastic plus creep strain through the cyclic life as a principal term in a damage equation. Manson, Halford and Hirschberg [17] separate the total strain into a time-dependent or creep, and time-independent or plastic parts. They find large differences in endurance depending on whether the creep is programmed in tensile or compressive positions in the cycle. Tensile creep followed by compressive plastic flow effects the most damaging combination, with tensile creep followed by compressive creep nearly as damaging. This would suggest that the tensile creep part of the total strain is the most damaging, most significant part. While these models address material behavior at creep temperatures, creep-like behaviors persist at room temperature for titanium, as most other structural alloys. The form of the stress-strain curve, most especially the strain hardening rate, directly affects its magnitude. Thus it could be useful to examine the effect of the inverted strain hardening of these titanium alloys on the room temperature creep strain as a damage criteria.

One way of estimating the cyclic creep strain involves a balancing of the stress relaxation at constant strain, occurring during dwell period of the cyclic load-time pattern, with the strain required to restore this stress by strain hardening, a subject developed Guiu and Pratt [18], following earlier work by Feltner [19] and Buck [20]. In what follows, the estimate is limited to the creep following the tensile plastic straining. Although with present symmetrical straining pattern the compressive creep strain would be of comparable extent, the partitioning results of Halford et al [17] would suggest the tensile creep the more damaging by far. Consider an axial load P on the specimen in terms of stress σ and area A

$$P = \sigma A \tag{4}$$

Differentiating

$$dP = \sigma dA + A d\sigma \tag{5}$$

For the creep condition, assume constant load or $dP = 0$. Partial constituents of the two differentials may be substituted. The areal differential is the Poisson contraction $\partial A_\nu = -A d\epsilon$, (i.e., assuming no volume change or $\nu = 0.5$). There are two stress partials. The partial of stress relaxation is taken as

$\theta\sigma_m = \sigma m \frac{d\dot{\epsilon}_p}{\dot{\epsilon}_p} = -\sigma m \frac{dt}{t}$, where m is the exponent of stress relaxation or strain rate sensitivity. Using the m exponent implies a linear relationship between log σ and log $\dot{\epsilon}$. This differs in form from the direct-stress dependency used by Guiu and Pratt [18]. However, since only small stress changes are involved, there is little difference between these forms. The partial of strain hardening is $\theta_p\, d\,\epsilon_p$. With this, Eq. 5 can be expressed in terms of a "creep strain" differential

$$d\epsilon_c \simeq m \frac{dt}{t} \left[\frac{\theta_p}{\sigma} - 1\right]^{-1} \tag{6}$$

where θ_p and σ are functions of the strain point at which they are measured in the cyclic stress-strain curve. Integrating over the dwell period of the load cycle, as explained in reference [11] gives

$$\Delta\epsilon_c = m \ln\left[1 + \frac{t_H}{t_L}\right] \left[\frac{\theta_p}{\sigma} - 1\right]^{-1} \tag{7}$$

where t_L and t_H are load and hold time of the load cycle, respectively, and $\Delta\epsilon_c$ is the tensile creep strain in each cycle.

In the present apparatus using a screw driven machine, head displacement rates are constant: a fixed rate during loading/ unloading; zero during head motion reversal. Elastic compliance in the system absorbs some of the head motion during rising load, reducing the strain rate of specimen material as though the loading time, t_L in Equation 7 had been increased. During the dwell with fixed head position, the load is not constant, as for proper creep, but decreases with the "creep" strain along a load line of (negative) slope equal to the effective system stiffness. Again following Guiu and Pratt [18] these considerations allow Equation 7 to be modified

$$\Delta\epsilon_c = m \ln\left[1 + \frac{t_H}{t_L(1 + \theta_T/M)}\right] \left[\frac{\theta_p}{\sigma} - 1 + \frac{M}{\sigma}\right]^{-1} \tag{8}$$

Here M is the effective elastic stiffness of everything in the load train, including the specimen; it is expressed as the stress change per unit strain. As noted in Section 3, this is about 13,000 MPa (2000 ksi) for this assemblage. Attempts to use the compliance-corrected expression of the Equation 8 have not been fruitful. The addition of the M/σ term greatly increases the strain excursion required to reach instability, ($\Delta\epsilon_c \rightarrow \infty$). As a compromise, a slight addition, dropping the coefficient from unity

to $\sqrt{3}/2$, as consistant with its value in earlier crack propagation modeling [11], has been applied for these calculations.

The first term of Equation (7) is constant for a given material and load cycle, and indeed varies little among these titanium alloys, which vary little in m value (Table III). Thus for data correlation one might initially compare only the last, shape-dependent, time-independent, term of Equation 7 with fatigue endurance. Regarding the creep strain as an increment of damage, LCF life may be compared to its inverse. An LCF life factor L is thus defined as

$$L \equiv \left[\frac{\theta_p}{\sigma} - \sqrt{3}/2\right] \tag{9}$$

where θ_p and σ, defined in Equations 1-3, are functions of the strain excursion.

7. LIFE FACTOR ESTIMATES FOR EACH SPECIMEN

Following the above rationale, values of L, the LCF Life Factor, are calculated from each test record. In Figure 6, the left hand end of each arrow is the value L_i based on the initial value of θ_p and σ, while the right hand arrow head L_e is based on equilibrium values, which reflect the inversion in strain hardening rate. In Figure 7, curves are fitted to the extremes are laid upon the data for crack initiation life (Figure 2). In cases where the ISH effect is small, the fit is close. Where it is large, the data tends to fit the L_e-curve at the higher cycle end, but then, cross over to the L_i-curve for the lower cycle end.

One reason for this cross over could be a greater influence of the damaging cycles inflicted early-on in the cyclic life before the ISH has evolved fully. In attempt to average the damage throughout the life, a "damage fraction" per cycle, defined as L^{-1}, was summed through the total cyclic life to initiation N_i,

$$\bar{L}^{-1} \equiv \frac{1}{N_i} \sum_{1}^{N_i} L(N)^{-1} \tag{10}$$

where $\bar{L}$ is an averaged LCF life factor. Here the shift in θ_T values was measured continuously from the cyclic stress strain records, and summed on a small programmable recording calculator, with results

shown in Figure 8. Not every cyclic loop was measured, except in the tests at large strain excursion, hence low cyclic life. Otherwise, 5 to 10 blocks of essentially similar shape were summed. This procedure is subject to the qualification that the limits of summation, the initiation life, is the measurement one seeks to predict; hence $\bar{L}$ is not fully independent of N_i. However, the influence of the limits is not dominant. With this said, the fit of $\bar{L}$ to N_i seems considerably improved. Another way of showing this is to plot $\bar{L}$ against N_i, Fig. 9, thus eliminating the strain excursion as an independent variable. The factor of proportionality between $\bar{L}$ and N_i, as determined by straight line fits, is recorded in Table III, and discussed later. These are essentially the same as the values derived from the methods of Figs. 7 and 8, the slight differences due the way of estimating L, and displaying data, and subjectivity of fitting the curves to the data.

8. LCF-LIFE FACTORS FROM A SINGLE CYCLIC CURVE

To the extent that the initial, small-envelope cyclic curve can be treated as a portion of a full-envelope cyclic curve, and that the strain hardening rate shift $\Delta\theta_p$ is constant, it should be possible to construct L_i and L_e limits from a single-cycle stress-strain curve. Examples of this, Figure 10, are taken from the grain size series of the 0.20 oxygen Ti-6Al-4V. Extrapolation to low cyclic strain excursion, which such a construction should allow, is needed to compare with stress-controlled fatigue data of greater fatigue life. The equilibrium-value L_e trend is calculated by adding the theta shift values $\Delta\theta_p$ from Figure 5 to each measurement value. These limits compare favorably with the L_i and L_e limits based on measurements in each individual LCF test, transferred from Figure 6. Hopefully, when referred to tensile stress excursion, they will compare usefully to the stress-controlled initiation data presently being gathered for these alloys in the NRL program. In comparisons in the range of higher initiation life, the effect of inverted strain hardening should be negligible. Here the fixed absolute difference in plastic strain hardening rate vanishes relative to the infinite values of θ_p approached in nearing the cyclic proportional limit.

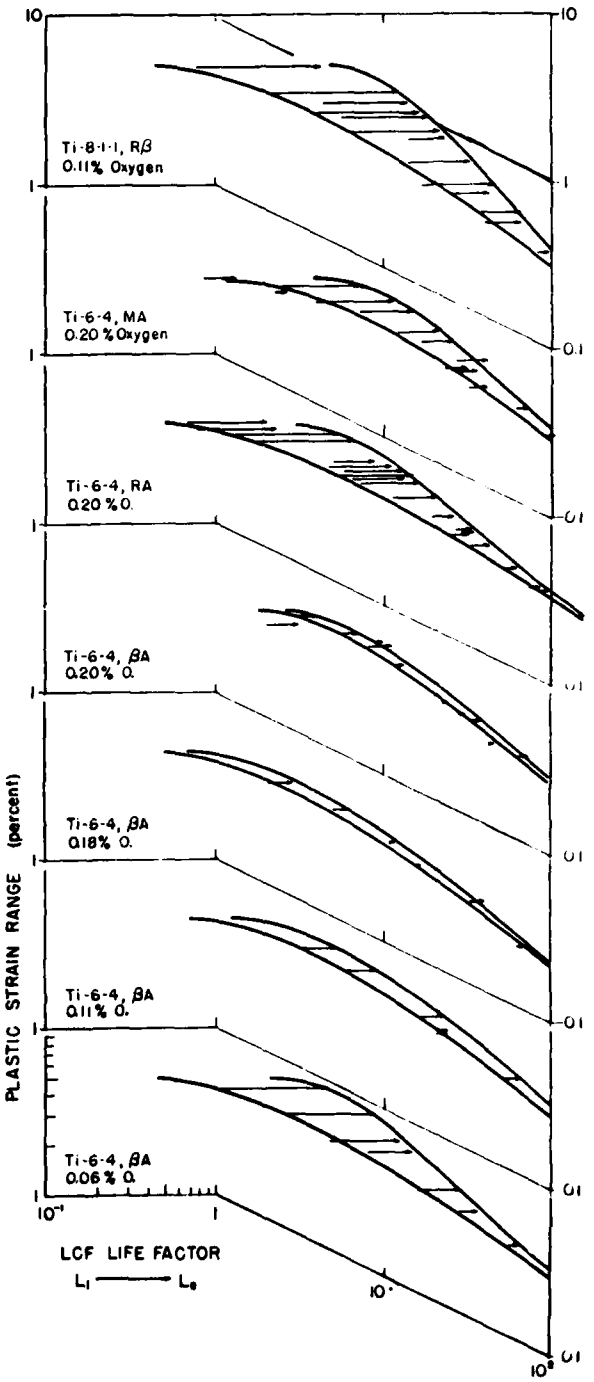

Figure 6 — Inversely proportional to the cyclic creep strain, an LCF life factor is calculated for initial vs, at arrowhead, equilibrium strain hardening rate.

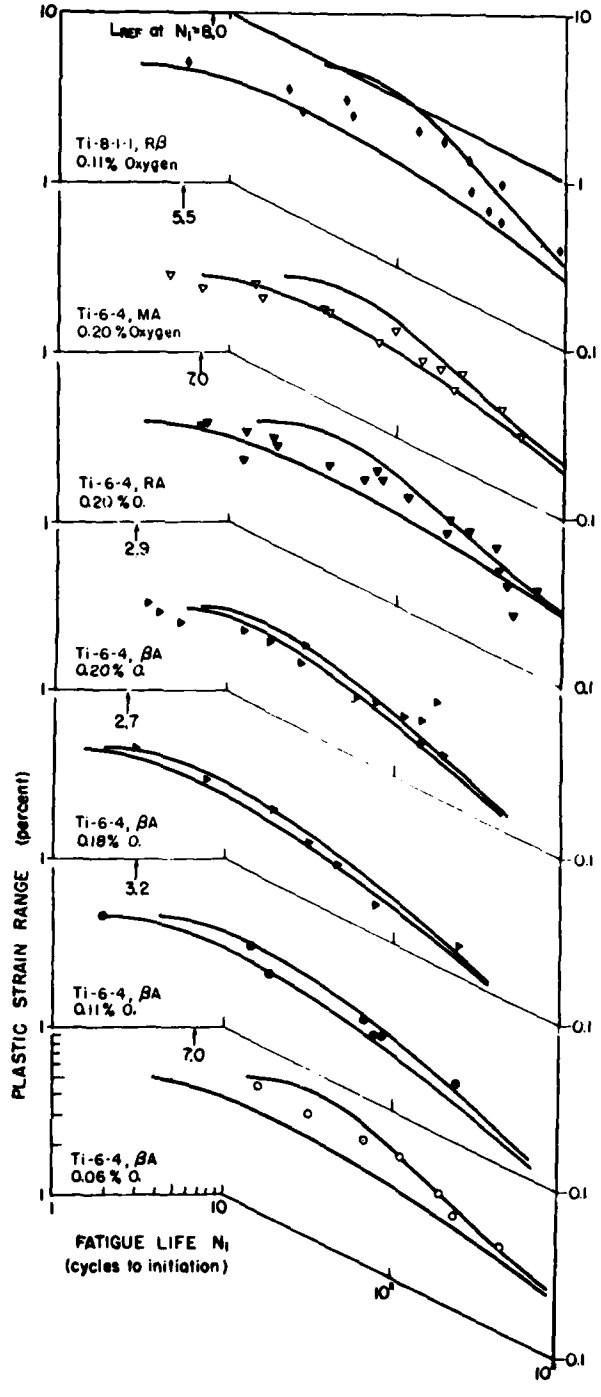

Figure 7 — The curves fitted through extremities of L-factor estimates of Figure 6, roughly bound measured fatigue life values.

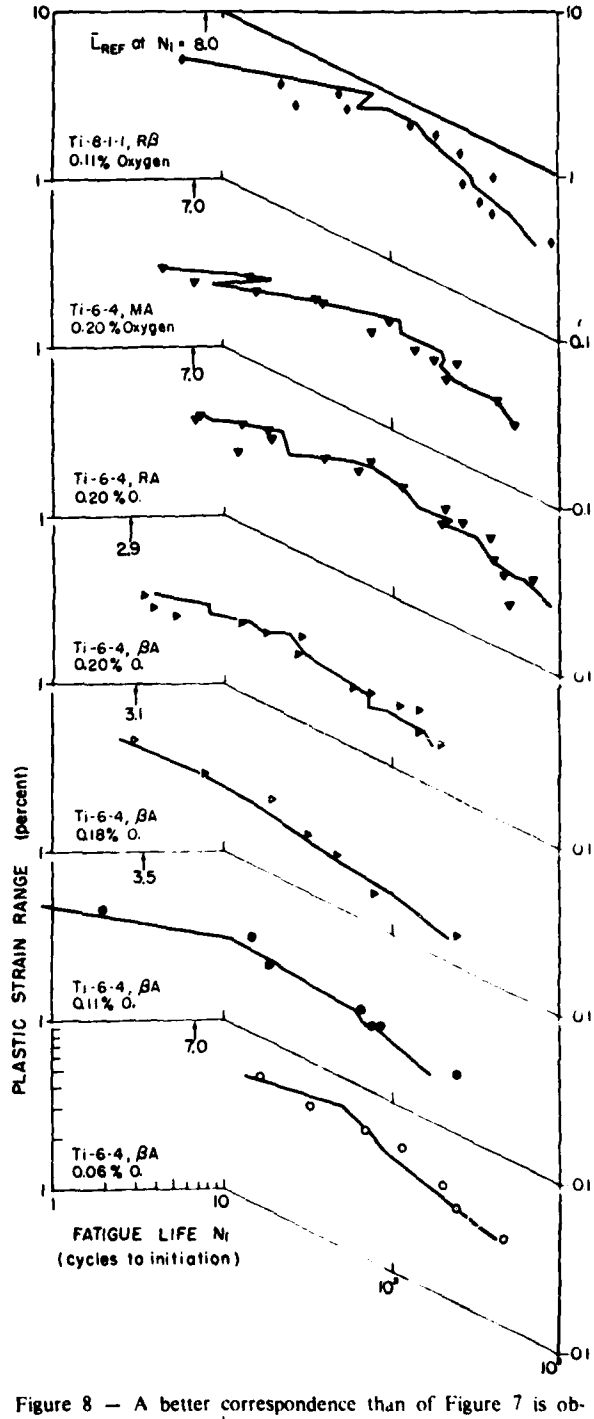

Figure 8 — A better correspondence than of Figure 7 is obtained by averaging L^{-1} values, as damage fractions, throughout the cyclic life.

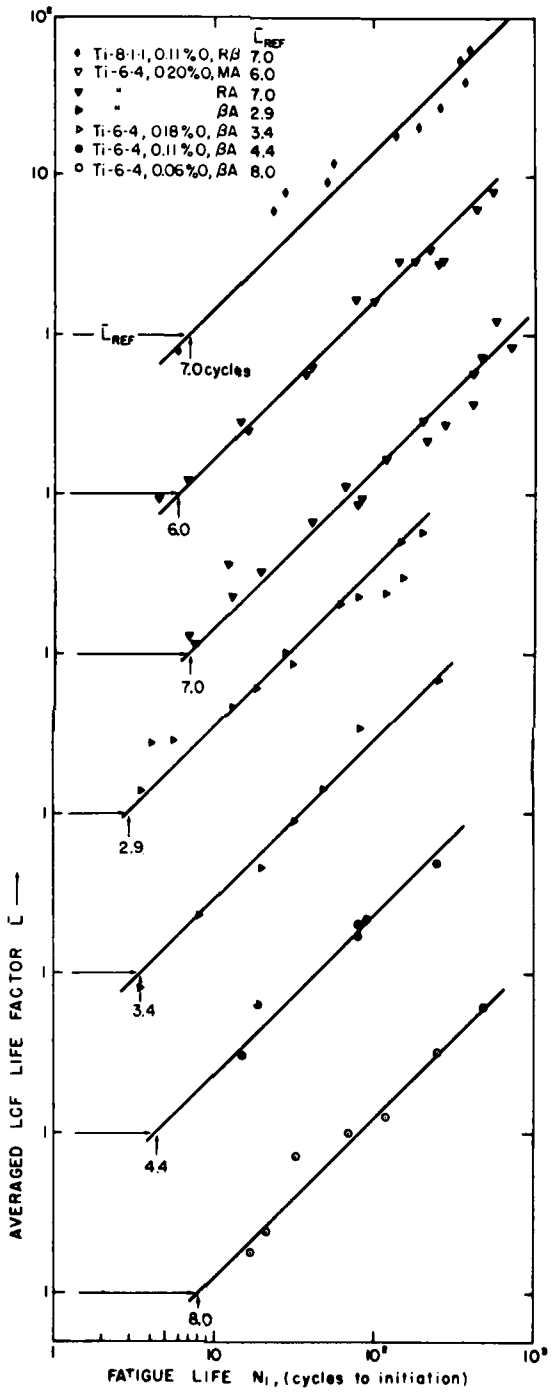

Figure 9 — The averaged LCF life factor of Figure 8 may be plotted directly vs initiation life, thus eliminating the strain excursion as the independent variable. The ratio of $\bar{L}/N_i$ is a measure of the materials resistance to crack ininiation once cyclic flow properties have been normalized.

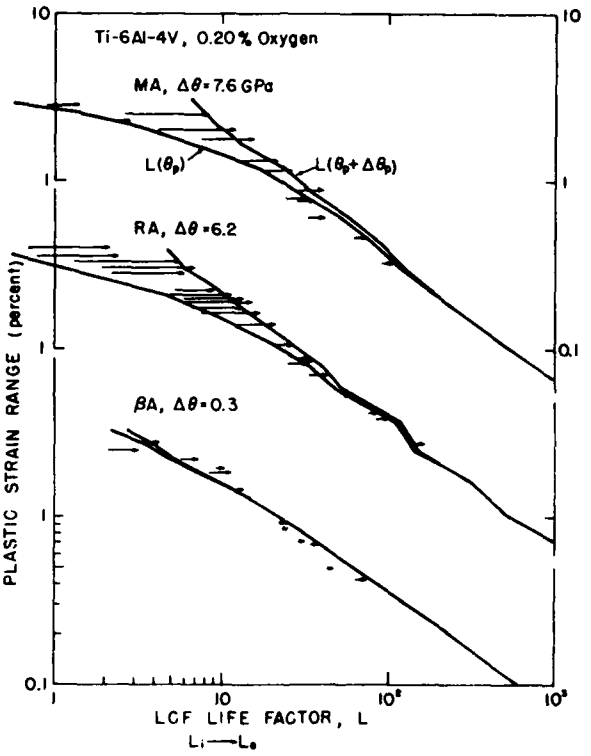

Figure 10 — Values of L from a full cyclic stress strain curve and for its θ_p-values augmented by its characteristic ISH shift $\Delta\theta_p$ from Figure 5, provide envelopes bounding L-limits in individual LCF tests from Figure 6.

9. CRITICAL CUMULATIVE CREEP STRAIN

The matching parameter $N_i/\bar{L}$ provides a measure of the cumulative creep strain for crack initiation ϵ_c. From Equation 7 this is given by

$$\epsilon_c = N_i \Delta \epsilon_c = m \ln \left[1 + \frac{t_H}{t_L}\right] \frac{N_i}{\bar{L}} \tag{11}$$

Values of the stress relaxation exponent, m, Table III, were measured in connection with earlier crack propagation modeling [11]; these range from 1.2 to 1.4×10^{-3}. For the roughly triangular wave form, $\ln[1 + t_H/t_L]$ should be the order of 0.1. Values of ϵ_c so calculated seem to correlate with the reduction in area of the monotonic tensile tests, as might be expected. However, the absolute values of ϵ_c are only the order of 10% of the reduction in area. Since it includes only the creep strain, and not the plastic strain excursion, this is not surprising. However, it seems unlikely that adding the cumulative plastic strain, without severe derating with respect to its damage potential, would improve the correlations. The fact that the critical cumulative creep strain is so varied means that the effect of inverted strain hardening accounts for only a part of the improved fatigue performance, principally for the convex shape of the data trend in the low cycle range.

The proposed dependency of fatigue life on cycle hold time has yet to be verified. For given cyclic strain excursion, material and temperature, ϵ_c, m and $\bar{L}$ of Eq. [11] may be considered constants. If we let x be the normalized hold time t_H/t_L, then $Ni \sim 1/\log(1 + x)$. The usual plot of log N_i vs log t_H should have the form of a plot of log $[1/\log(1 + x)]$ vs log x. Such a plot curves downward with diminishing slope: roughly -0.55 for t_H/t_L from 1 to 10; -0.23 from 10 to 10^3; and -0.1 from 10^3 to 10^6. Independently of temperature, stress relaxation exponent, and strain excursion, such a curve would appear to fit much of the high temperature hold-time data compiled by Krempl and Wundt [21]. Thus, it might well be found to fit room temperature hold-time data on present alloys.

Readers familiar with earlier work of this writer on crack propagation modeling [11] will recognize his prior use of the cyclic creep strain criterion. In crack propagation, it is taken to control the environmentally-independent portion of the crack extension in each cycle. Here the strain (hardening) required to offset stress relaxation at the crack tip is viewed as driven by crack extension, rather than by

the stored elastic energy in the fatigue loading apparatus. The dual roles emphasize the general importance of plastic flow properties in processes of fracture and fatigue.

10. CONCLUSIONS

From this study of the strain-controlled cyclic deformation of alloys from the Ti-6Al-4V and Ti-8Al-1Mo-1V systems, of diverse microstructure and oxygen contents, is is concluded that:

1. An inversion in cyclic strain hardening rate is observed by which the terminal equilibrium value exceeds the initial value of true plastic strain hardening rate.

2. This inversion or "theta shift" $\Delta\theta_p$ is constant for a given titanium alloy, independent of the cyclic strain excursion.

3. In the 5-500 cycle range, resistance to fatigue crack initiation tends to increase with the value of $\Delta\theta_p$.

4. This effect of $\Delta\theta_p$ on the fatigue crack initiation resistance is modeled in terms of a cyclic creep strain damage criterion.

11. ACKNOWLEDGMENTS

The LCF tests were performed by C. L. Lamb, who persevered through the days preceding his recent NRL retirement in order to complete them. No work of any consequence could have been done without the generous aid of G. R. Yoder in supplying materials and metallurgical expertise. Discussions with T. W. Crooker have been most helpful. Finally, the funding of the Naval Air Systems Command and the Office of Naval Research is gratefully acknowledged.

12. REFERENCES

1. Yoder, G. R., Cooley, L. A., and Crooker, T. W. (1977), "Enhancement of Fatigue Crack Growth and Fracture Resistance in Ti-6Al-4V and Ti-6Al-6V-2Sn Through Microstructural Modification,"

J. Engineering Materials and Technology, 99, 313-318. (See also NRL Report 8049, November 1976).

2. Yoder, G. R., Cooley, L. A. and Crooker, T. W., (1978) "Fatigue Crack Propagation Resistance of Beta Annealed Ti-6Al-4V Alloys of Differing Interstitial Oxygen Content," Met. Trans. A., 9A, 1413-1420. (See Also NRL Report 8166, October 1977).

3. Yoder, G. R., Cooley, L. A. and Crooker, T. W., (1979) "Improvement of Environmental Crack Propagation Resistance in Ti-8Al-1Mo-1V Through Microstructural Modification" NRL Memo Report 3955, March 1979.

4. Feltner, C. E. and Beardmore, P., (1971), "Strengthening Mechanisms in Fatigue" in *Achievement of High Fatigue Resistance in Metals* ASTM STP 467, 77-112.

5. Boettner, R. C., Laird, C., and McEvily, A. J., (1965) "Crack Nucleation and Growth in High Strain-Low Cycle Fatigue" Trans. Metallurgical Society AIME, 233, 379-387.

6. Abdel-Raouf, H., Topper, T. H. and Plumtree, A., (1973) "Effects of Grain Size and Temperature on the Cyclic Strength and Fracture of Iron," *Fatigue of Elevated Temperatures*, ASTM STP 520, 300-310.

7. Beevers, C. J. and Robinson, J. L., (1969) "Some Observations on the Influence of Oxygen Content on the Fatigue Behavior of α-Titanium," J. Less-Common Metals, 17, 345-352.

8. "Tentative Recommended Practice for Constant-Amplitude Low-Cycle Fatigue Testing" E606, Annual Book of ASTM Standards, published annually.

9. "Tentative Method of Test for Plane-Strain Fracture Toughness of Metallic Materials" E399, Annual Book of ASTM Standards, published annually.

10. Coffin, L. F., Jr., and Taveonelli, J. F., (1959), "The Cyclic Straining and Fatigue of Metals," Trans. Metal. Soc., AIME 215, 794-807.

11. Krafft, J. M., (1980) "Case Studies of Fatigue Crack Growth Using an Improved Micro-Ligament Instability Model," NRL Memo Report 4161, January 1980.

12. Raske, D. T. and Morrow, Jo Dean, (1969), "Mechanics of Materials in Low Cycle Fatigue Testing," *Manual on Low Cycle Fatigue Testing*, ASTM STP 465, 1-25.

13. Wells, C. H. and Sullivan, C. P., (1969) "Low Cycle Fatigue Crack Initiation in Ti-6Al-4V," Trans. Am. Soc. Metals 62, 263-270.

14. Stolz, R. E. and Pelloux, R. M. (1976) "The Bauschinger Effect in Precipitation Strengthened Aluminum Alloys," Met. Trans. 7A, 1295-1306.

15. Richman, R. H. and Landgraf, R. W., (1975), "Some Effects of Retained Austenite on the Fatigue Resistance of Carburized Steel," Met. Trans. 6A, 955-964.

16. Serensen, S. V., Schneiderovitch, R. M. and Gusenkov, A. P., (1973), "Kinetic Deformation Criteria of Cyclic Fracture at High Temperature," *Fatigue at Elevated Temperatures*, ASTM STP 520, 670-677.

17. Halford, G. R., Hirschberg, M. H. and Manson, S. S. (1973), "Temperature Effects on the Strain Range Partitioning Approach for Creep Fatigue Analysis," *Fatigue at Elevated Temperatures*, ASTM STP 520, 658-669.

18. Guiu, F. and Pratt, P. L., (1964), "Stress Relaxation and the Plastic Deformation of Solids," Phys. Stat. Sol. 6, 111-120.

19. Feltham, P. (1961), "Stress Relaxation in Copper and Alpha-Brasses at Low Temperatures," J. Inst. Metals 89, 210-214.

20. Buck, O., (1964), "Mechanische Relaxation von Kupfer-Einkristallen," Phys. Stat. Sol. 3, 111-120.

21. Krempl, E. and Wundt, B. M., (1971), *Hold-Time Effects in High-Temperature Low-Cycle Fatigue*, ASTM STP 489.